Estimating the arterial input function from dynamic contrast-enhanced MRI data with compensation for flow enhancement (I)

Theory, method, and phantom experiments

van Schie, Jeroen; Lavini, Cristina; van Vliet, Lucas; Vos, Frans

DOI
10.1002/jmri.25906

Publication date
2017

Document Version
Final published version

Published in
Journal of Magnetic Resonance Imaging

Estimating the Arterial Input Function From Dynamic Contrast-Enhanced MRI Data With Compensation for Flow Enhancement (I): Theory, Method, and Phantom Experiments

Jeroen J.N. van Schie, PhD,[1] Cristina Lavini, PhD,[2] Lucas J. van Vliet, PhD,[1] and Frans M. Vos, PhD[1,2]*

Background: The arterial input function (AIF) represents the time-dependent arterial contrast agent (CA) concentration that is used in pharmacokinetic modeling.
Purpose: To develop a novel method for estimating the AIF from dynamic contrast-enhanced (DCE-) MRI data, while compensating for flow enhancement.
Study Type: Signal simulation and phantom measurements.
Phantom Model: Time–intensity curves (TICs) were simulated for different numbers of excitation pulses modeling flow effects. A phantom experiment was performed in which a solution (without CA) was passed through a straight tube, at constant flow velocity.
Field Strength/Sequence: Dynamic fast spoiled gradient echo (FSPGRs) at 3T MRI, both in the simulations and in the phantom experiment. TICs were generated for a duration of 373 seconds and sampled at intervals of 1.247 seconds (300 timepoints).
Assessment: The proposed method first estimates the number of pulses that spins have received, and then uses this knowledge to accurately estimate the CA concentration.
Statistical Tests: The difference between the median of the estimated number of pulses and the true value was determined, as well as the interquartile range (IQR) of the estimations. The estimated CA concentrations were evaluated in the same way. The estimated number of pulses was also used to calculate flow velocity.
Results: The difference between the median estimated and reference number of pulses varied from –0.005 to –1.371 (corresponding IQRs: 0.853 and 48.377) at true values of 10 and 180 pulses, respectively. The difference between the median estimated CA concentration and the reference value varied from –0.00015 to 0.00306 mmol/L (corresponding IQRs: 0.01989 and 1.51013 mmol/L) at true values of 0.5 and 8.0 mmol/l, respectively, at an intermediate value of 100 pulses. The estimated flow velocities in the phantom were within 10% of the reference value.
Data Conclusion: The proposed method accurately corrects the MRI signal affected by the inflow effect.
Level of Evidence: 1
Technical Efficacy: Stage 1

J. MAGN. RESON. IMAGING 2018;47:1190–1196.

The arterial input function (AIF) represents the time-dependent arterial contrast agent (CA) concentration, which is used in pharmacokinetic (PK) modeling of dynamic imaging data. Obtaining an accurate AIF is essential for accurate estimation of the PK model parameters. Dynamic contrast-enhanced magnetic resonance imaging (DCE-MRI) often uses a fast spoiled gradient echo (FSPGR) sequence, for which a theoretic relationship exists between the CA concentration and the

View this article online at wileyonlinelibrary.com. DOI: 10.1002/jmri.25906

Received Jun 6, 2017, Accepted for publication Oct 3, 2017.

*Address reprint requests to: F.M.V., Lorentzweg 1, Delft, The Netherlands. E-mail: f.m.vos@tudelft.nl

From the [1]Quantitative Imaging Group, University of Technology Delft, The Netherlands; and [2]Department of Radiology and Nuclear Medicine, Academic Medical Center Amsterdam, The Netherlands

Additional supporting information may be found in the online version of this article

signal enhancement, assuming that the magnetization resulting from the repeated application of RF pulses is in a steady state.[1,2] Therefore, the AIF is often directly computed from the signal measured in an artery close to the tissue of interest.[3]

This assumption does not hold, however, for spins in flowing blood, as they have not spent enough time in the field of view (FOV) to reach the steady state. Neglecting this can cause a biased estimate of CA concentration, which is detrimental to the estimation of PK parameters.[4] The effect manifests itself as a reduction of the signal enhancement, especially at high CA concentrations or for a low number of received pulses. In addition, T_2^* decay also has a nonlinear effect on the relation between concentration and signal. While choosing a very short echo time can reduce this effect, it causes a bias in the AIF, if not corrected for.[5,6]

The AIF can be obtained in several ways. The easiest approach is to use a population-averaged parameterized model.[7] Despite its simple implementation, this model ignores intersubject variations. It has been shown that the use of a subject-specific AIF improves the robustness of PK analysis.[8]

When deriving a subject-specific AIF from the DCE-MRI data, the measured arterial signal needs to be converted to CA concentration. It was proposed that the relation between the concentration and signal intensity could be calibrated with a flow phantom before performing the DCE-MRI scan.[9] This produces an unbiased AIF, but needs to be recalibrated for each imaging sequence, and is sensitive to susceptibility differences. It is therefore quite unpractical.

Various authors derive the CA concentration assuming a linear relation between signal intensity and CA concentration.[10–12] This is valid for low concentrations, but not with higher concentrations, in which case it leads to less accurate estimation of PK parameters. Other researchers use the full nonlinear relation between signal intensity and CA concentration, which provides a better estimate of the AIF,[13,14] and in turn improves the accuracy of the PK parameter estimates.[15] Such nonlinear conversion requires prior knowledge of the T_1 time of blood, which can either be measured in a separate scan, or acquired from the literature.[16]

Both the linear and the nonlinear conversion methods assume that the measured magnetization is in a steady state, which may not be true. The error introduced by this assumption depends on the number of excitation pulses that the spins have received. Although measuring at a downstream location can minimize this effect, this can still be insufficient.[17]

The purpose of this study was to develop a novel method for estimating the AIF from DCE-MRI data, while compensating for flow enhancement.

Materials and Methods

Correction Method

The developed method takes into account the spin dynamics during the transient state of an FSPGR sequence, including a correction for T_2^* decay. In order to estimate the AIF, the amount of enhancement due to the inflow effect is estimated first. Subsequently, the estimated amount of enhancement due to flow is compensated as the signal intensity is converted into concentration. A detailed description of the method can be found in the Supplementary Material, which also contain all the equations to which we refer.

Experimental Design

Two experiments were performed to assess the proposed method's ability to accurately and precisely estimate an AIF from DCE-MRI data. 1) The method was tested on simulated data, in order to quantify its accuracy and precision in estimating the number of pulses (Supplemental Eq. 13), and the CA concentration (Supplemental Eq. 15). 2) The theoretical behavior of spin dynamics in transient state (Supplemental Eq. 4) was verified in a controlled phantom experiment.

Simulation

ESTIMATING THE NUMBER OF PULSES. To assess the proposed method's accuracy and precision in estimating the number of pulses n, it was applied to a simulated set of signal-ratio curves. These arterial signal-ratio curves were created by generating a time–concentration curve (TCC) by means of Supplemental Eq. 9, with parameters $\boldsymbol{\theta}$ describing the population-averaged arterial TCC, as in Orton et al.[18] The TCCs were generated for a duration of 373 seconds and sampled at intervals of 1.247 seconds (300 timepoints). Next, the TCC was converted into time–intensity curves (TICs) through Supplemental Eq. 4. These TICs were generated for different values of n ranging from 10 to 200 in steps of 10. Thereby, the repetition time (TR) and echo time (TE) were set to 2.9 and 1.8 msec, respectively, the flip angle α was set to 15°, and the T_1 value of blood was assumed to be 1.779 seconds.[16] The simulated contrast agent was gadobutrol, of which a longitudinal relaxivity $r_1 = 4.1$ L/mmol/s and a transverse relaxivity $r_2^* = 6.5$ L/mmol/s was assessed at 3T.[2] All these MRI settings were identical to the settings of a patient study, which is described in Part II of this article.[19] Subsequently, Gaussian white noise with an signal-to-noise ratio (SNR) of 20 was added. The TICs were then divided by their average precontrast signal to obtain signal-ratio curves. This was repeated 500 times for each value of n, each time with different noise realizations. Each signal-ratio curve was then processed by the proposed method; see Fig. 1 for a schematic overview of the simulations. The difference between the median of the estimated values for n and the true value was considered a measure of the method's accuracy. The interquartile range of the estimated values of n was taken as a measure of the precision.

ESTIMATING THE CONCENTRATION. Similarly, Supplemental Eq. 15 was applied to a known set of concentrations to quantify the influence of an error in the estimated value of n on the subsequently estimated concentrations. Therefore, a set of concentrations ranging from 0 to 8 mmol/L, in steps of 0.5 mmol/L, was converted to signal ratio by means of Supplemental Eq. 6, using a fixed number of pulses n. The same MRI settings were used as described in the previous subsection. Next, 200 perturbed values n_{est} were generated around the true n through the method described in in the Theory section of the Supplemental material.

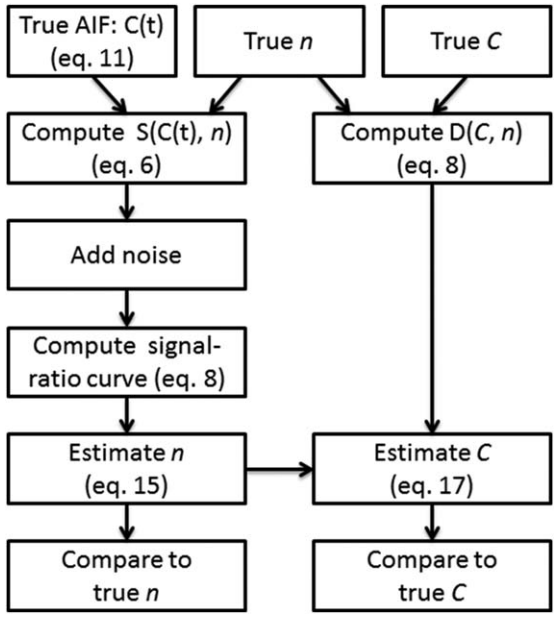

FIGURE 1: Flowchart of the simulations. The left column describes the procedure to estimate the number of pulses *n*, while the right column describes the procedure to estimate the concentration *C*.

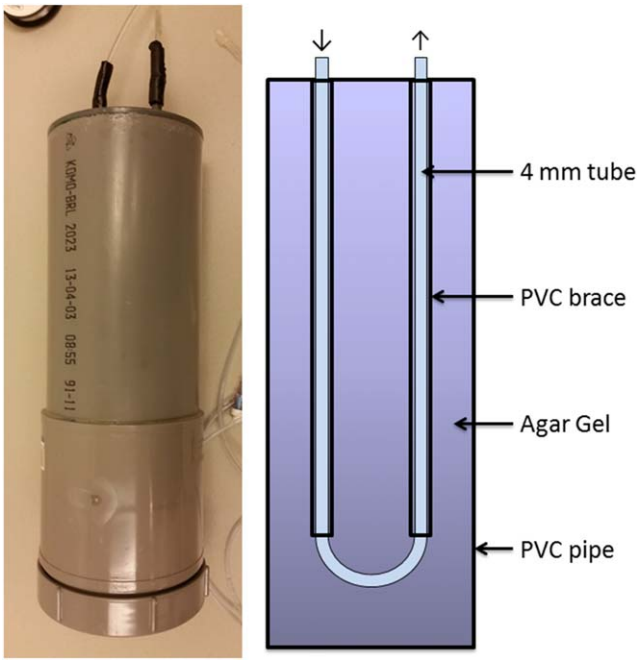

FIGURE 2: Left: Photograph of the flow phantom. Right: Schematic overview of the internal structure of the flow phantom (top view). The arrows at the top indicate flow direction.

Finally, the concentrations were estimated by solving Supplemental Eq. 15 for each of the combinations of true concentration and generated n_{est}. A new set of n_{est} was generated for each concentration, to ensure statistical independence. This procedure was performed eight times, with n set to 10, 40, 70, 100, 130, 160, 190, and 220 (see Fig. 1). The error in the estimated concentrations was assessed in the same manner as indicated in the previous paragraph.

Phantom Experiment

In order to test the validity of the model describing the signal generated by spins in transient state (Supplemental Eqs. 3 and 4), a phantom experiment was performed. A liquid consisting of copper sulphate diluted in 0.9% saline water was passed through a straight tube, at constant flow velocity v, while being scanned. This should ensure a linear relation between the distance along the tube d and the number of pulses perceived by the spins: $n = d/(v \cdot TR)$. The velocity could be estimated by substituting this expression into Supplemental Eqs. 3 and 4 and fitting it to the signal values measured along the tube. The validity of Supplemental Eq. 4 would indeed imply that the flow velocity can be correctly calculated from the estimated number of pulses n.

Specifically, the phantom consisted of a flexible plastic tube (4 mm inner diameter) passing through two small, rigid braces of PVC (each 300 mm long), forming a U-tube. The PVC braces were mounted onto the lid of a larger PVC pipe (125 mm inner diameter), with the flexible plastic tube ends extending through the lid. The remaining space inside the larger PVC pipe was filled with agar gel doped with copper sulphate (20 g/kg agar powder, 2 mmol/L $CuSO_4$) to reduce discontinuities in magnetic susceptibility, essentially mimicking tissue surrounding a blood vessel (see Fig. 2).

Despite the differences in viscosity between blood and water, the plastic tube's small inner diameter was expected to ensure laminar flow with a Reynolds number similar to that of blood flowing through the abdominal aorta. An empty IV-bag was filled with 500 ml of this fluid.

First, the IV-bag was scanned with an inversion recovery (IR) sequence, allowing determination of the T_1 value of the fluid (T_I = 50, 100, 300, 1000, 1500 msec, TR = 7000 msec, TE = 5.3 msec, FOV = 167 × 167 × 25 mm^3, matrix size = 336 × 336 × 10 voxels). This T_1 value is required to reliably estimate the velocity by fitting Supplemental Eq. 4 to the tubes' signal profiles. The T_1-value of the fluid was determined by fitting the theoretical relationship between the IR signal intensity and T_1 to the measured IR data, using a nonlinear least-squares regression algorithm implemented in MatLab (v. R2014b; MathWorks, Natick, MA).

Subsequently, the IV-bag was connected to the inlet tube of the phantom, and suspended 1.20 m above the outlet tube. The tubes inside the phantom were filled with fluid, and the flow was stopped. The phantom was then scanned with a dynamic FSPGR sequence ($\alpha = 15°$; TR = 2.9 msec; TE = 1.8 msec; FOV = 200 × 200 × 75 mm^3; matrix size = 128 × 128 × 30 voxels; no partial Fourier; no parallel imaging; scan time = 250 sec; 100 timepoints). The phantom was scanned axially, so that the tubes were positioned perpendicular to the slices. This was done to ensure that no spins outside the FOV would be excited. After ~30 seconds of scanning the stationary fluid, the flow restriction was removed and the fluid was allowed to flow freely under the influence of gravity. During this period, the discharge of fluid was measured using a stopwatch and a graduated beaker, providing a reference estimate of the average flow velocity in the tubes.

The left and right segments of the U-tube were manually segmented from the dynamic series, by selecting two points on the centerline towards the ends of both segments. Subsequently, all voxels with a radial distance smaller than 2 mm to the lines

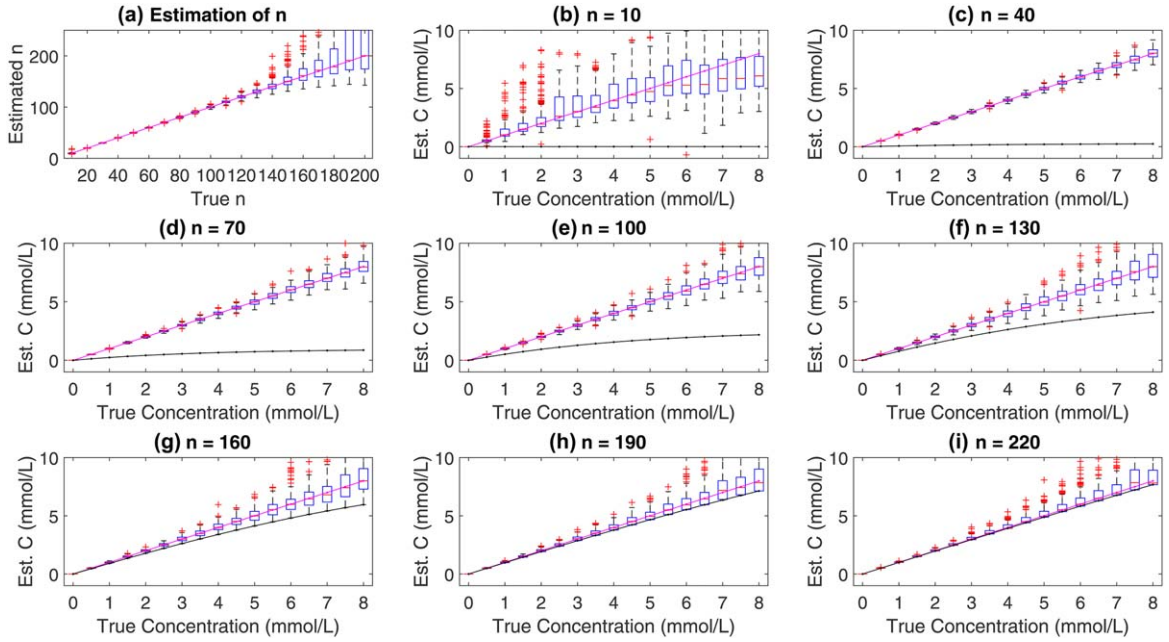

FIGURE 3: Simulation results. (a) Estimated number of pulses *n* for true *n* ranging from 10 to 200. (b–i) Estimated concentrations for true *C* ranging from 0 to 8 mmol/L, for *n* = 10 to 220 in steps of 30, respectively. In all plots, boxes indicate 25/50/75th percentile, whiskers extend to 1.5 times the interquartile range, red crosses show outliers. The magenta line indicates unity. The black line shows the estimated concentration when assuming *n* = 8.

between the points were taken to represent the tube content, and the distance d of the included voxels along the tube was computed. The intensity profile along the tubes was extracted for three different time intervals: before flow, during flow, and after flow. Then the theoretical signal relation for spins in transient state (Supplemental Eqs. 3 and 4, substituting $n = d/(v \cdot TR)$) was fitted to each of these profiles. One minor change was made to this signal relation, in that the behavior of spins outside the FOV was also included in the model. This was done by assuming that a single additional flip angle pulse α_{pre} preceded the sequence. This would account for any partial saturation the spins may have before entering the FOV. Particularly, the initial condition used for deriving Supplemental Eq. 3 was changed to $M_z\ (n=0) = M_0\ \cos(\alpha pre)$, resulting in:

$$a = M_0\left(\cos(\alpha_{pre}) - \frac{1-E_1}{1-\cos(\alpha)E_1}\right)$$

The inclusion of this effective prepulse should only be necessary for the second (right) tube segment, where the spins' longitudinal magnetization may not have relaxed back to equilibrium after being excited in the first (left) tube segment. After the effective prepulse, the spins flow through the FOV with velocity v, producing exponentially decaying signal intensity along the tube. Fitting the model to the signal measured in both tube segments gave an estimate for v (as well as M_0 and α_{pre}). This estimate was compared to the reference velocity.

Results

Simulation Results

The results of the Monte Carlo simulations estimating the number of pulses n by means of Supplemental Eq. 13 is shown in Fig. 3a. Furthermore, the outcome of the experiments estimating the concentrations through Supplemental Eq. 15, for five settings of n, is shown in Fig. 3b–i. For reference, the estimated concentration assuming $n = \infty$ is also shown in Fig. 3b–i.

It is clearly visible that estimating the concentration while wrongfully assuming $n = \infty$ results in a marked underestimation of the concentration, especially at lower values of n and at higher concentrations.

The exact differences between the true and the median estimated number of pulses, concentrations are respectively separately plotted in Fig. 4a,b. Additionally, the interquartile ranges of the estimations of the concentrations are plotted separately in Fig. 4c,d. Clearly, the estimation uncertainty increases when the true concentration increases, although the relation between the uncertainty and the number of pulses is more complicated.

Phantom Experiment Results

The average velocity of the fluid passing through the phantom, as measured with a graduated beaker and stopwatch, was found to be 21 cm/s.

The T_1-value of the fluid, estimated in a manually selected region of interest in a T_1-map produced using an IR sequence, was 1071.8 ± 9.4 msec.

False-colored images acquired with the dynamic FSPGR sequence before, during, and after flow are shown in Fig. 5. The enhanced signal intensity due to flow is clearly visible in the middle row, especially in the left tube segment. The intensity profiles along the tube segments for

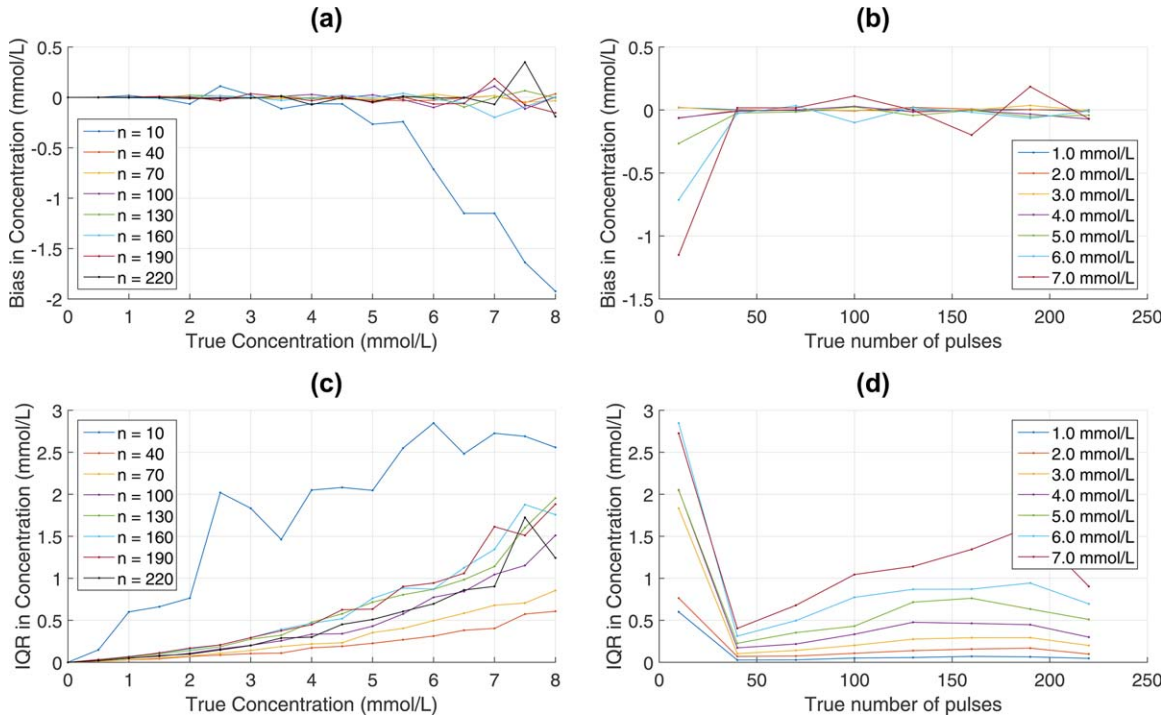

FIGURE 4: Differences (a) between true and median estimated number of pulses and (b) between true and median estimated concentrations, both as a function of the true number of pulses. Furthermore, interquartile ranges in estimated concentrations, (c) for different number of pulses *n*, (d) for different concentrations are shown.

each time interval are shown in Fig. 6. The decaying exponential behavior of the signal during flow (cf. Supplemental Eq. 4) is clearly visible. Additionally, the signal shows marked enhancement on the inflow sides of the tubes. Reversely, there is reduced signal intensity further downstream (compared to the stationary case), which we attribute to the mixing of spins with different velocities. These spins will have different phase encodings within a voxel, and therefore slightly cancel each other out. We hypothesize that this effect occurs everywhere along the tubes in the same way. As such, it also affects the head. However, one cannot see this because in the head the signal is dominated by the enhancement due to the inflowing unsaturated spins. Furthermore, the signal intensity on the inflow side in the right tube is lower than on the inflow side of the left tube, because the spins have not fully relaxed to equilibrium after being excited in the left tube.

Figure 6 also shows the result of fitting the theoretical model for the physical behavior of the spins (Supplemental Eq. 4) to the measured data. For the left tube, the estimated velocity was 191.5 mm/s, while the effective prepulse was negligibly small. For the right tube, the estimated velocity was 189.9 mm/s, and the effective prepulse 10.64°. Observe that both estimated velocities are within 10% of the reference value.

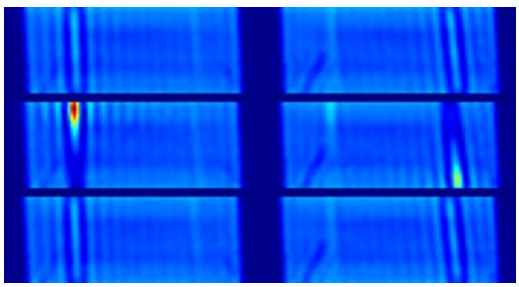

FIGURE 5: Acquisitions of the phantom before flow (top row), during flow (middle row), and after flow (bottom row), at two slice positions through the phantom. Fluid flows downwards in the left tube (middle left) and upwards in the right tube (middle right), showing the inflow effect.

Discussion

Our results show that our flow correction method is accurate (able to reproduce the true number of pulses and concentration) and precise (robust in the presence of noise) when applied to the simulated and phantom data.

The increased spread in the estimation of n with larger number of pulses in the simulations is the result of the fact that increasing the number of pulses brings the MR signal closer to the steady state. This hinders the estimation, as the signal intensity no longer depends on n. Furthermore, the spread in the estimated concentrations increases with increasing C due to the MR signal leveling off at higher concentrations. Therefore, the signal intensity no longer relates to the CA concentration, which decreases the precision of the estimates.

For very low true values of n, the effect of CA on the MRI signal is very small, so that noise has a large effect on the estimation of C. At medium true values of n (around 80 pulses), the derivative of the signal ratio with respect to

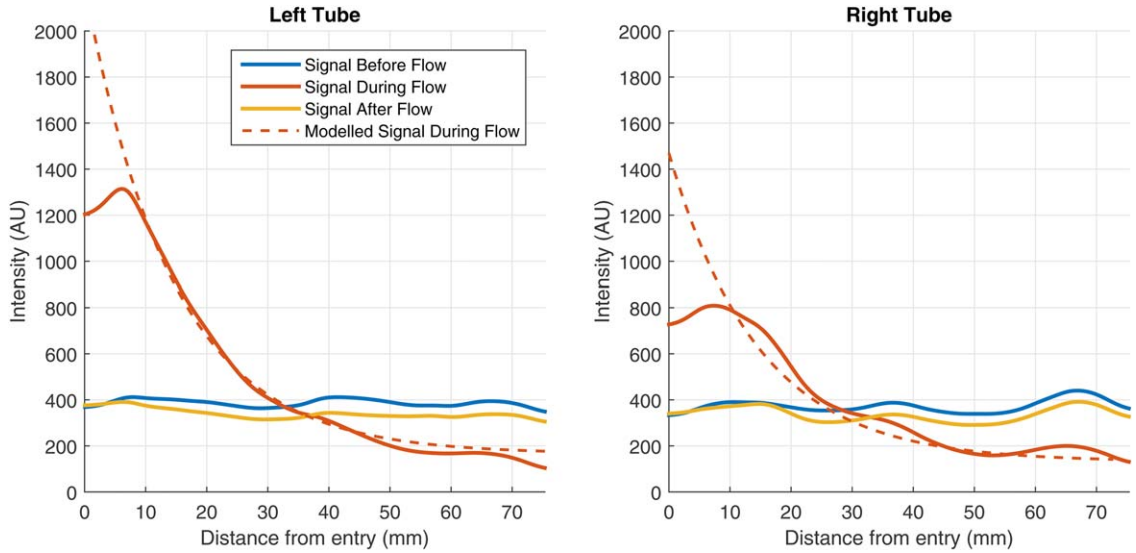

FIGURE 6: Solid lines: intensity profiles along both tube segments, for time intervals before, during, and after flow. Dashed lines: theoretical model fitted to the measured signal during flow.

n is large, which translates to a low spread in C. Then at higher true values of n (around 150 pulses), the spread in the estimated values of n, and thereby the spread in C, increases. Finally, when the spins reach steady state, the effect of errors in the estimated values of n have less influence on the estimation of C, and the spread decreases again.

Thus, the proposed method requires moderate levels of CA (within the physiologically expected range), as is the case with any method for deriving the concentration from the signal intensity.

The experiment with the flow phantom demonstrates that the measured intensities behave, indeed, according to the presented theory of spin dynamics in transient state.

Previously, the arterial CA concentration has been calculated assuming a linear relationship between concentration and signal enhancement.[10–12] Currently, however, the theoretical nonlinear relation between signal intensity and CA concentration is more often applied to do so,[3] since this improves the accuracy of the PK parameter estimates.[15] The nonlinear conversion requires prior knowledge of the T_1 time of blood, which can either be measured in a separate scan, or acquired from the literature.[16]

The severe effects that flow can have on the quantification of the CA concentration in DCE-MRI has been widely observed.[6,9,17,20] Essentially, different issues affect the signal from spoiled GRE sequences that are conventionally applied: the space-dependent variation of the RF, partial volume effects,[21] incomplete spoiling,[22] and a restriction in the amount of the RF pulses that are experienced by the spins due to flow.[17]

The mentioned linear and the nonlinear CA conversion methods both assume that the measured magnetization is in a steady state, which may not be true for flowing spins. Although measuring at a downstream location can minimize this effect,[7,17,20] this approach can still be insufficient and may not always be feasible.

Our method essentially applies the nonlinear conversion of signal into CA concentration, while taking into account the spin dynamics during the transient state of an FSPGR sequence, including a correction for T_2^* decay. In order to do so it is assumed that the AIF's profile follows Orton et al's AIF model.[18] Effectively, the estimated amount of enhancement due to flow is compensated as the signal intensity is converted into concentration.

As an alternative to our approach, one might consider setting up a full minimization equation including all concentrations to be estimated simultaneously (cf. Supplemental Eq. 6) while using the AIF model fit as a constraint. However, this leaves an unstable minimization problem since it requires simultaneous estimation of 300 concentrations (for each timepoint), five AIF model parameters and one parameter representing the number of pulses from only 300 data points. To create a stable minimization problem we essentially constrained the number of pulses through the first step of our approach.

We did not investigate the effect of the flip angle on the precision and accuracy of AIF estimation. It can be foreseen that an increased flip-angle enhances T_1-weighting, which is preferred for a linear relation between signal magnitude and the contrast agent concentration. Simultaneously, however, it yields lower SNR and increased specific absorption rate (SAR). Our choice of 15° is a compromise between sufficient T_1-weighting and short acquisition time. We experienced that SAR limits required an extension of TR at higher flip angles on our scanner, effectively resulting in less T_1-weighting and longer acquisition time. We consider an investigation of the effect of the flip angle on AIF estimation beyond the scope of the current study.

A limitation of the proposed experiment follows from constraining the area under the bolus peak to a fixed value as it is described in the supplementary material,

(Supplemental Eqs. 11 and 12). A different setting might introduce a change in the estimation of n, and therefore in the estimation of C. However, it was reported by Parker et al that the relative standard error in the model parameter corresponding to the area under the bolus peak is only 5.4%.[7] This suggests that there is indeed little variation in a_B among people. One can foresee that the assumption is violated in patients with cardiac disease, however. If cardiac output could be measured in such patients, then the method might still be applicable as a_B is adjusted based on Supplemental Eq. 11. Clearly, such an extension requires further research.

Another limitation of the method is that noise on the MR signal can introduce errors in the estimation of C. It is therefore beneficial if the method is applied to the signal from several voxels simultaneously, so that a median AIF can be computed. Clearly, this may require alignment of the data. Finally, the MR signal is a function not only of the number of pulses, but also of the amplitude of the perceived excitation pulses (the B_1-field). The effects of an inhomogeneous B_1-field can easily be included in the proposed model, however, if the B_1-field is calibrated.

In conclusion, we have presented a method to estimate and correct for flow enhancement that can affect the estimation of the AIF. The simulations show that the proposed method 1) sustains accurate estimation of the perceived number of pulses by flowing spins; 2) uses this information to accurately quantify the concentration of contrast agent. Furthermore, the flow phantom experiment demonstrates that spins in a transient state indeed produce the expected signal intensity: decaying exponentially with increased number of pulses. It confirms that the proposed approach is in agreement with the theory.

Acknowledgment

Contract grant sponsor: European Union's Seventh Framework Programme; contract grant number: FP7/2007-2013: VIGOR++ Project that was sponsored through the EU's 7th framework programme (grant agreement no. 270379).
We thank Ron Hoogerheide for the construction of the flow phantom.

References

1. Fram EK, Herfkens RJ, Johnson GA, et al. Rapid calculation of T1 using variable flip angle gradient refocused imaging. Magn Reson Imaging 1987;5:201–208.
2. Stalder AF, von Elverfeldt D, Paul D, Hennig J, Markl M. Variable echo time imaging: Signal characteristics of 1-M gadobutrol contrast agent at 1.5 and 3T. Magn Reson Med 2008;59:113–123.
3. Schabel MC, Parker DL. Uncertainty and bias in contrast concentration measurements using spoiled gradient echo pulse sequences. Phys Med Biol 2008;53:2345–2373.
4. Roberts C, Little R, Watson Y, Zhao S, Buckley DL, Parker GJ. The effect of blood inflow and B(1)-field inhomogeneity on measurement of the arterial input function in axial 3D spoiled gradient echo dynamic contrast-enhanced MRI. Magn Reson Med 2011;65:108–119.
5. De Naeyer D, Debergh I, De Deene Y, Ceelen WP, Segers P, Verdonck P. First order correction for T2*-relaxation in determining contrast agent concentration from spoiled gradient echo pulse sequence signal intensity. J Magn Reson Imaging 2011;34:710–715.
6. Wang H, Cao Y. Correction of arterial input function in dynamic contrast-enhanced MRI of the liver. J Magn Reson Imaging 2012;36:411–421.
7. Parker GJ, Roberts C, Macdonald A, et al. Experimentally-derived functional form for a population-averaged high-temporal-resolution arterial input function for dynamic contrast-enhanced MRI. Magn Reson Med 2006;56:993–1000.
8. Rijpkema M, Kaanders JH, Joosten FB, van der Kogel AJ, Heerschap A. Method for quantitative mapping of dynamic MRI contrast agent uptake in human tumors. J Magn Reson Imaging 2001;14:457–463.
9. Ivancevic MK, Zimine I, Montet X, et al. Inflow effect correction in fast gradient-echo perfusion imaging. Magn Reson Med 2003;50:885–891.
10. Zollner FG, Zimmer F, Klotz S, Hoeger S, Schad LR. Renal perfusion in acute kidney injury with DCE-MRI: deconvolution analysis versus two-compartment filtration model. Magn Reson Imaging 2014;32:781–785.
11. Taouli B, Johnson RS, Hajdu CH, et al. Hepatocellular carcinoma: perfusion quantification with dynamic contrast-enhanced MRI. AJR Am J Roentgenol 2013;201:795–800.
12. Lim SW, Chrysochou C, Buckley DL, Kalra PA, Sourbron SP. Prediction and assessment of responses to renal artery revascularization with dynamic contrast-enhanced magnetic resonance imaging: a pilot study. Am J Physiol Renal Physiol 2013;305:F672–678.
13. Jensen RL, Mumert ML, Gillespie DL, Kinney AY, Schabel MC, Salzman KL. Preoperative dynamic contrast-enhanced MRI correlates with molecular markers of hypoxia and vascularity in specific areas of intratumoral microenvironment and is predictive of patient outcome. Neuro Oncol 2014;16:280–291.
14. Rajan S, Herbertson L, Bernardo M, Choyke P. A dialyzer-based flow system for validating dynamic contrast enhanced MR image acquisition. Magn Reson Med 2014;72:41–48.
15. Aronhime S, Calcagno C, Jajamovich GH, et al. DCE-MRI of the liver: effect of linear and nonlinear conversions on hepatic perfusion quantification and reproducibility. J Magn Reson Imaging 2014;40:90–98.
16. Shimada K, Nagasaka T, Shidahara M, Machida Y, Tamura H. In vivo measurement of longitudinal relaxation time of human blood by inversion-recovery fast gradient-echo MR imaging at 3T. Magn Reson Med Sci 2012;11:265–271.
17. Garpebring A, Wirestam R, Ostlund N, Karlsson M. Effects of inflow and radiofrequency spoiling on the arterial input function in dynamic contrast-enhanced MRI: a combined phantom and simulation study. Magn Reson Med 2011;65:1670–1679.
18. Orton MR, d'Arcy JA, Walker-Samuel S, et al. Computationally efficient vascular input function models for quantitative kinetic modelling using DCE-MRI. Phys Med Biol 2008;53:1225–1239.
19. van Schie JJN, Lavini C, van Vliet LJ, et al. Estimating the arterial input function from dynamic contrast-enhanced MRI data with compensation for flow enhancement (II): Applications in spine diagnostics and assessment of Crohn's disease. J Magn Reson Imaging 2017 (In Press).
20. Cheng H-LM. T1 measurement of flowing blood and arterial input function determination for quantitative 3D T1-weighted DCE-MRI. J Magn Reson Imaging 2007;25:1073–1078.
21. van Osch MJP, van der Grond J, Bakker CJG. Partial volume effects on arterial input functions: Shape and amplitude distortions and their correction. J Mag Reson Imaging 2005;22:704–709.
22. Yarnykh VL. Optimal radiofrequency and gradient spoiling for improved accuracy of T1 and B1 measurements using fast steady-state techniques. Magn Reson Med 2010;63:1610–1626.